9º Congresso Nacional de Mecânica Experimental
Aveiro, 15-17 de Out., 2014

Vibroacoustic Analysis of Plates with Damping Patches Using a Layerwise Theory and the Rayleigh-Ritz Method

Amorim, J. [1,2]; Dias Rodrigues, J. [2]

[1] INEGI – Instituto de Engenharia Mecânica e Gestão Industrial
[2] Departamento de Engenharia Mecânica, Faculdade de Engenharia da Universidade do Porto

ABSTRACT

This work addresses issues on vibration and noise control studying an efficient model to simulate the dynamic and vibroacoustic behavior of plates with constraining-layer damping patches. The proposed model, gathers the advantages of the layerwise models with the number of degrees of freedom of a single-layer theory. In addition, the Rayleigh-Ritz method arises as a reliable alternative to the finite element method and offers a very efficient solution regarding patches handling. Taking advantage of the resourceful solutions that this model offers the efficiency of the damping treatments is analyzed and discussed.

1- INTRODUCTION

1.1 - The Present Model

Nowadays, the vibrational and acoustic properties of high performance structures are increasingly considered as key constraints in automotive, railway or aerospace industries during the design process. Beyond the structural integrity of these structures, the public realization of the importance of noise as a major pollution and annoyance source has grown as well as the sound quality notion among the choice criteria. However, with the increasing strong demands of more efficient and reliable structures, engineers need to develop refined and more accurate models of complex multilayer structures with damping technologies.

The major objective of this work is implement a theory, firstly developed by Guyader and Lesueur (1978) and later formulated by Woodcock (2008), to model laminate structures. The proposed model, gathers the advantages of the layerwise models with the number of degrees of freedom of a single-layer theory. In addition, the use of the Rayleigh-Ritz method ensures a much easier viscoelastic patches handling, once that it works at an energetic level. This methodology is a main objective of this work once that the use of constrained-layer damping (CLD) treatments can be improved by the use of partial treatments (Fig. 1), which decrease the structural modification in the host structure, decrease the added mass and enable a selective damping.

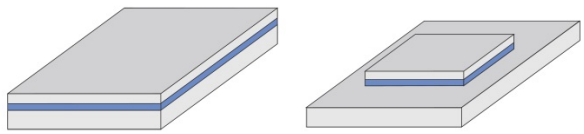

a) Classical CLD b) CLD Patch

Fig. 1 – Total and partial viscoelastic treatments.

2- STRUCTURAL MODEL

2.1 - Multi-Layer of Hybrid Type

The proposed model uses a piecewise linear displacement field across the thickness where the displacement continuity is satisfied and the shear stresses continuity is enforced at each interface. The practical result is that the displacement field of each layer $\ell\,[2,\cdots,\mathrm{N}]$ is linked to the displacement field of the first layer, leading to a five unknown mechanical model where

all the unknowns are the unknowns of the first layer.

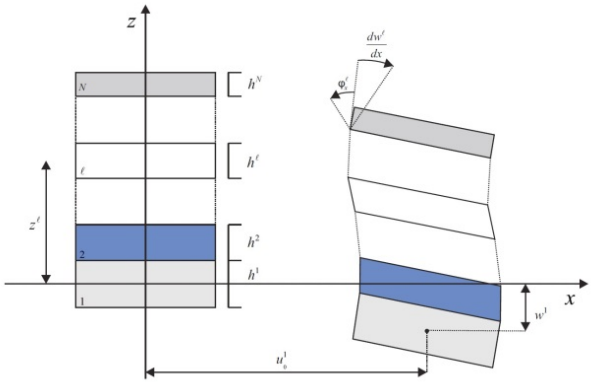

Fig. 2 – Displacement field of a multilayered material.

The displacement field of each layer is written as:

$$u^{\ell}(x,y,z) = u_0^{\ell}(x,y,z^{\ell}) + (z^{\ell} - z)\left(\frac{\partial w^{\ell}(x,y)}{\partial x} + \varphi_x^{\ell}(x,y)\right)$$
$$v^{\ell}(x,y,z) = v_0^{\ell}(x,y,z^{\ell}) + (z^{\ell} - z)\left(\frac{\partial w^{\ell}(x,y)}{\partial y} + \varphi_y^{\ell}(x,y)\right)$$
$$w^{\ell}(x,y,z) = w^{1}(x,y) \tag{1}$$

where $\ell \in [1,...,N]$ is the number of the layer, w is the transverse displacement, u_0^{ℓ} and v_0^{ℓ} are the in-plane (membrane) displacements along x and y directions and φ_x^{ℓ} and φ_y^{ℓ} are the rotations caused by shear effects around x and y directions in layer ℓ, respectively. The z^{ℓ} is z-coordinate of the midplane of the layer ℓ and connects all the upper layers to the first one. The adopted strain field is given by:

$$\varepsilon_{ij}^{\ell} = \frac{1}{2}\left(\frac{\partial u_i^{\ell}}{\partial x_j} + \frac{\partial u_j^{\ell}}{\partial x_i}\right), \text{for i = j}$$
$$\gamma_{ij}^{\ell} = \frac{1}{2}\left(\frac{\partial u_i^{\ell}}{\partial x_j} + \frac{\partial u_j^{\ell}}{\partial x_i}\right), \text{for i} \neq \text{j} \tag{2}$$

where $u_{i,j}^{\ell}$ and $x_{i,j}$, respectively, denote $u^{\ell}, v^{\ell}, w^{\ell}$ and x, y, z when subscript i, j takes values x, y, z. As in many others plate theories, a generalized plane stress $\sigma_{zz}^{\ell} = 0$ is assumed. However, the assumed displacement field in Eq. (1) leads to $\varepsilon_{zz}^{l} = 0$, which is not compatible with the generalized plane stress assumed. Nevertheless, the low values of ε_{zz}^{ℓ} compared with other strains allows this kind of displacement field. In the context of a general modeling for the orthotropic properties and considering that orthotropic axes coincide with the natural axes of the plate, the stresses and the deformations are related by:

$$\begin{Bmatrix} \sigma_{xx}^{\ell} \\ \sigma_{yy}^{\ell} \\ \tau_{xy}^{\ell} \\ \tau_{xz}^{\ell} \\ \tau_{yz}^{\ell} \end{Bmatrix} = \begin{bmatrix} C_{1111}^{\ell} & C_{1122}^{\ell} & 0 & 0 & 0 \\ C_{1122}^{\ell} & C_{2222}^{\ell} & 0 & 0 & 0 \\ 0 & 0 & C_{1212}^{\ell} & 0 & 0 \\ 0 & 0 & 0 & C_{1313}^{\ell} & 0 \\ 0 & 0 & 0 & 0 & C_{2323}^{\ell} \end{bmatrix} \begin{Bmatrix} \varepsilon_{xx}^{\ell} \\ \varepsilon_{yy}^{\ell} \\ 2\gamma_{xy}^{\ell} \\ 2\gamma_{xz}^{\ell} \\ 2\gamma_{yz}^{\ell} \end{Bmatrix} \tag{3}$$

where:

$$C_{1111}^{\ell} = E_x^{\ell} / (1 - \nu_{xy}^{\ell}\nu_{yx}^{\ell})$$
$$C_{1122}^{\ell} = E_y^{\ell}\nu_{xy}^{\ell} / (1 - \nu_{xy}^{\ell}\nu_{yx}^{\ell})$$
$$C_{2222}^{\ell} = E_y^{\ell} / (1 - \nu_{xy}^{\ell}\nu_{yx}^{\ell})$$
$$C_{1212}^{\ell} = G_{xy}^{\ell}$$
$$C_{1313}^{\ell} = G_{xz}^{\ell}$$
$$C_{2323}^{\ell} = G_{yz}^{\ell} \tag{4}$$

Here, E_x^{ℓ} and E_y^{ℓ} are Young's modulus in x and y directions, G_{xy}^{ℓ} and G_{xz}^{ℓ} are the transverse shear modulus, G_{xy}^{ℓ} is the shear modulus in the O_{xy} plane, and ν_{xy}^{ℓ} and ν_{yx}^{ℓ} are the Poisson's ratios of the layer ℓ. This model uses a piecewise linear displacement field across the thickness where the displacement continuity is satisfied and the shear stresses continuity is enforced at each interface. These conditions link the displacement fields of each layer to the base layer, regardless the number of

layers. The conditions of displacement at each interface are written as:

$$\begin{aligned} u^{\ell}(x,y,z^{\ell}+\frac{h^{\ell}}{2}) &= u^{\ell+1}(x,y,z^{\ell+1}-\frac{h^{\ell+1}}{2}) \\ v^{\ell}(x,y,z^{\ell}+\frac{h^{\ell}}{2}) &= v^{\ell+1}(x,y,z^{\ell+1}-\frac{h^{\ell+1}}{2}) \\ w^{\ell}(x,y,z) &= w^{1}(x,y) \end{aligned} \quad (5)$$

The following equations express the shear stress continuity at each interface:

$$\begin{aligned} \tau_{xz}(x,y,z^{\ell}+\frac{h^{\ell}}{2}) &= \tau_{xz}(x,y,z^{\ell+1}-\frac{h^{\ell+1}}{2}) \\ \tau_{yz}(x,y,z^{\ell}+\frac{h^{\ell}}{2}) &= \tau_{yz}(x,y,z^{\ell+1}-\frac{h^{\ell+1}}{2}) \end{aligned} \quad (6)$$

which allows to write the displacement field of the layer ℓ with the one of the first layer, recursively:

$$\mathbf{Y}^{\ell} = \mathbf{\Omega}^{\ell}\mathbf{\Omega}^{\ell-1}\ldots\mathbf{\Omega}^{2}\mathbf{Y}^{1} = \widehat{\mathbf{\Omega}}^{\ell}\mathbf{Y}^{1} \quad (7)$$

where:

$$\mathbf{Y}^{\ell} = [u_0^{\ell}, v_0^{\ell}, \partial w^{\ell}/\partial x, \partial w^{\ell}/\partial y, \varphi_x^{\ell}, \varphi_y^{\ell}]^{\mathrm{T}} \quad (8)$$

and matrix $\widehat{\mathbf{\Omega}}^{\ell}$ is defined in Guyader and Leseuer (1978) and is a matrix that allow one to write the global motion of a multilayered material in terms of the displacement of the first layer.

2.2 - Variational Principle and the Rayleigh-Ritz Method

The equations of motion are derived from the Lagrange-d'Alembert variational principle and for the present case, considering the undamped problem, it consists on solving the equation:

$$\delta\int_{t_1}^{t_2}\mathcal{L}(q^i,\dot{q}^i)\mathrm{d}t + \int_{t_1}^{t_2} Q_i^{ext}\delta q^i \mathrm{d}t = 0 \quad (9)$$

where $\mathcal{L}(q^i,\dot{q}^i)$ is the Lagragian operator and is given by:

$$\mathcal{L}(q^i,\dot{q}^i) = T - V \quad (10)$$

where T and V are, respectively, the kinetic and deformation energy of the plate, q^i and $\dot{q}^i$ are the generalized displacements and velocities, respectively, and Q_i^{ext} are the generalized external forces.

In this work, the patch handling is done solving Eq. (9) for any virtual displacement δq^i and bringing all the deformation effects back to the base layer, defining a surface energy density. The Lagragian term is divided in two parts corresponding to the covered and the uncovered parts:

$$\begin{aligned} \delta\int_{t_1}^{t_2}\left(\int_{S_u}(e_t^s - e_v^s)\mathrm{d}S + \int_{S_c}(e_t^d - e_v^d)\mathrm{d}S\right)\mathrm{d}t \\ + \int_{t_1}^{t_2} Q_i^{ext}\delta q^i \mathrm{d}t = 0 \end{aligned} \quad (11)$$

where S_i is the surface with $i = u$ for the uncovered part and $i = c$ for the covered part, e_t^j and e_v^j are, respectively, the surface density of kinetic energy and the surface density of deformation energy for the multilayered material j, with $j = s$ for the support (base layer) material, and $j = d$ for the damped (all the layers) material.

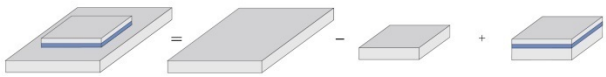

Fig. 3 – Superposition principle in the patch handling.

To make the patch's handling possible at an energetic level, the kinetic and deformation energy of the covered part must include the contribution of the base layers. Therefore, the energy of the common layers to covered and uncovered parts is retired from the energy of the entire uncovered plate. Then the total contribution of the covered part is added, as shown in Fig. 3.

The kinetic energy of each part, uncovered and covered, is now easily calculated from the surface density of kinetic energy of multilayered material as:

$$e_t^j = \frac{1}{2}\sum_{\ell=1}^{N^j}\int_{-\frac{h^{\ell,j}}{2}}^{\frac{h^{\ell,j}}{2}} \rho^{\ell,j}\,|\dot{\mathbf{u}}^{\ell,j}|^2\,\mathrm{d}(z^{\ell}-z) \quad (12)$$

where $\rho^{\ell,j}$ is the density of the layer ℓ of the multilayered material j and $|\dot{\mathbf{u}}^{\ell,j}|^2$ is the square of the velocity field modulus. The

surface density of deformation energy of each part, required for the calculation of the deformation energy V is given by:

$$e_v^j = \frac{1}{2}\sum_{\ell=1}^{N^j}\int_{-\frac{h^{\ell,j}}{2}}^{\frac{h^{\ell,j}}{2}} \sigma_{ik}^{\ell,j}\varepsilon_{ik}^{\ell,j}\mathrm{d}(z^\ell - z) \qquad (13)$$

where $\sigma_{ik}^{\ell,j}$ and $\varepsilon_{ik}^{\ell,j}$ represent here, respectively, the normal and shear stresses and strains from the constitutive model defined in Eq. (3).

This methodology is possible due to the Rayleigh-Ritz method where the domain is explicitly discretized (the approximation functions are globally defined) in opposition, for example, to the finite element method where the domain is implicitly discretized. The equations of motion are obtained solving Eq. (11) for a generalized displacement variation δq^i, which takes the form:

$$\left\{\delta q^i\right\} = \left\{\delta w,\ \ \delta u_0,\ \ \delta v_0,\ \ \delta\varphi_x,\ \ \delta\varphi_y\right\} \qquad (14)$$

Once that Lagrange's equations cannot be solved in general for any displacement variation, in this study a Rayleigh-Ritz method is used. This method requires a function basis for the expansion of the five different unknowns, where the trial functions need to satisfy the geometric boundary conditions. In this work, a trigonometric basis of functions with sine and cosine functions is considered. This basis has a maximum order m for the x direction and a maximum order n for the y direction. As an example, for a simply supported plate the transverse displacement takes the form:

$$\begin{aligned} w(x,y,t) &= \sum_{\substack{1\le p\le m\\ 1\le q\le n}} A^{pq}(t)\phi_w^{pq} \\ &= \sum_{\substack{1\le p\le m\\ 1\le q\le n}} A^{pq}(t)\sin\left(\frac{p\pi x}{a}\right)\sin\left(\frac{q\pi y}{b}\right) \end{aligned} \qquad (15)$$

In the preceding equation, the coefficient $A^{pq}(t)$ is time-dependent and if the same methodology is used for the remaining generalized displacements the coefficients $A^{pq}(t)$, $B^{pq}(t)$, $C^{pq}(t)$, $D^{pq}(t)$, $E^{pq}(t)$ can be stacked up to build a global $5\times m\times n$ vector $\mathbf{X}(t)$ of unknowns given by:

$$\left\{\mathbf{X}(t)\right\} = \begin{Bmatrix}\mathbf{A}(t)\\ \mathbf{B}(t)\\ \mathbf{C}(t)\\ \mathbf{D}(t)\\ \mathbf{E}(t)\end{Bmatrix} = \begin{Bmatrix}A^{11}(t)\\ \vdots\\ \vdots\\ E^{mn}(t)\end{Bmatrix} \qquad (16)$$

Eq. (11) can now be solved introducing the overall coefficient vector $\mathbf{X}(t)$ and the external forces work, leading to:

$$\delta\int_{t_1}^{t_2}\mathcal{L}(\{\mathbf{X}\},\{\dot{\mathbf{X}}\})\mathrm{d}t + \int_{t_1}^{t_2}\{\mathbf{F}\}^{\mathrm{T}}\{\delta\mathbf{X}\})\mathrm{d}t = 0 \qquad (17)$$

where $\{\mathbf{F}\}$ is the generalized discrete external force vector. Solving Eq. (17) leads to Lagrange's equation for the components of the generalized displacements X_j:

$$\frac{\mathrm{d}}{\mathrm{d}t}\frac{\partial T}{\partial \dot{X}_j} - \frac{\partial V}{\partial X_j} = F_j \qquad (18)$$

Applying the Lagrange's equations to each unknown, a linear system of $(5\times m\times n)$ differential equations for the forced motion in a matrix form is obtained:

$$[\mathbf{M}]\{\ddot{\mathbf{X}}(t)\} + [\mathbf{K}]\{\mathbf{X}(t)\} = \{\mathbf{F}(t)\} \qquad (19)$$

where $[\mathbf{M}]$ is the mass matrix, $[\mathbf{K}]$ the stiffness matrix and $\{\mathbf{F}(t)\}$ the external force vector. For harmonic solicitations of a given angular frequency ω, and considering the damping properties by means of complex material properties as well as the frequency dependence of the mass and stiffness matrices, the system takes the form:

$$(-\omega^2[\mathbf{M}(\omega)] + [\widetilde{\mathbf{K}}(\omega)])\{\widetilde{\mathbf{X}}\} = \{\widetilde{\mathbf{F}}\} \qquad (20)$$

where the tilde denotes the complex variables. In Eq. (20) the frequency dependence of the stiffness matrix is highlighted. This is a common feature in models that are used to simulate structures with viscoelastic treatments once that the

viscoelastic materials are defined by their complex modulus which is frequency dependent. However, in Eq. (20) is also shown that the mass matrix is frequency dependent. This is a particular characteristic of this model and at first sight is a surprising characteristic once that the density of viscoelastic materials isn't frequency dependent. Nevertheless, it is well know that the mass matrix is a function of the integration over the thickness of the velocity field which in turn is the time derivative of the displacement field. As was seen before the displacement field of a generic layer ℓ is written in function of the unknowns of the first layer due to the enforced shear stress continuity at each interface which makes the displacement field a function of the relations between the shear moduli of consecutive layers. Therefore, once that the viscoelastic materials are defined by their complex shear modulus, Eq. (21), the mass matrix is also frequency dependent.

$$\begin{aligned}\tau(\omega) &= \tilde{G}(\omega)\gamma(\omega) \\ &= [G'(\omega) + \mathrm{j}G''(\omega)]\gamma(\omega)\end{aligned} \tag{21}$$

where $\tilde{G}(\omega)$ is the complex shear modulus, $G'(\omega)$ is the storage shear modulus and represent the real part of the complex modulus and $G''(\omega)$ is the loss shear modulus and represents the imaginary part of the complex modulus. It's not surprising that the velocity field varies with frequency once that the displacement field of the viscoelastic layer depends on its mechanical properties experiencing a larger displacement when the material is more flexible. To understand this frequency dependence, the mass matrix cannot be seen exclusively as a property of the system but rather as a measure of the kinetic energy.

2.3 - External Force Vector

Remembering Eq. (17) the virtual work done by the external forces is given by:

$$\int_{t_1}^{t_2} \{\mathbf{F}\}^{\mathrm{T}} \{\delta \mathbf{X}\} \mathrm{d}t \tag{22}$$

If the generalized force vector is related with the displacements vector $\mathbf{X}(t)$ and its components, then it can be written as:

$$\left\{\tilde{\mathbf{F}}\right\} = \left\{\tilde{\mathbf{F}}_w \tilde{\mathbf{N}}_x \tilde{\mathbf{N}}_y \widetilde{\mathbf{M}}_x \widetilde{\mathbf{M}}_y\right\} \tag{23}$$

where $\tilde{\mathbf{F}}$ is the normal loading, $\tilde{\mathbf{N}}_x$ and $\tilde{\mathbf{N}}_y$ are the generalized in-plane tensions and $\widetilde{\mathbf{M}}_x$ and $\widetilde{\mathbf{M}}_y$ are the generalized bending moments. In this work, only the transverse load is considered which leads to the following generalized force vector:

$$\left\{\tilde{\mathbf{F}}\right\} = \begin{Bmatrix} \tilde{\mathbf{F}}_w \\ \mathbf{0} \\ \mathbf{0} \\ \mathbf{0} \\ \mathbf{0} \end{Bmatrix} \tag{24}$$

where the transverse load is given by:

- Pressure Load:

$$\{\tilde{\mathbf{F}}_w\} = \int_0^a \int_0^b \tilde{P}(x,y)\{\phi_{\mathbf{w}}(x,y)\}\mathrm{d}y\mathrm{d}x \tag{25}$$

- Punctual Excitation:

$$\{\tilde{\mathbf{F}}_w\} = \tilde{f}\{\phi_{\mathbf{w}}(x_0,y_0)\} \tag{26}$$

where $\tilde{P}(x,y)$ is the applied pressure in the plate, $\tilde{f}$ is the point force applied and (x_0,y_0) is the point where this force is applied.

VIBROACOUSTIC MODEL

2.4 - Plane Wave

The vibroacoustic model is based on the model developed by Loredo et al. (2011), which considers the plate separated by two semi-infinite fluid media.

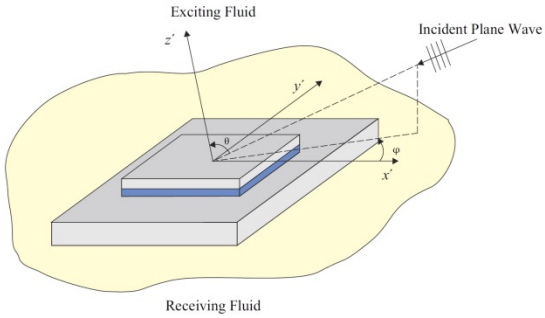

Fig. 4 – Patched plate submitted to a plane wave.

The plane wave represented in Fig. 4 causes forces acting on the plate due to the difference of pressure existing in the two sides. It is assumed light fluid for the two sides of the plate and with this assumption the pressure caused by the radiation impedance of the fluid mediums can be neglected. In Loredo et al. (2011) an evaluation of the fluid load importance was made. They showed that, for the studied case, the fluid-structure coupling was weak, neglecting it for all their studies even when the thickness and the density of the considered plates were different.

Considering these assumptions, the incident pressure field generated by the incident plane wave can be written as:

$$\tilde{P}_{\text{inc}}(x,y) = 2\,\tilde{p}_{\text{inc}} e^{-\text{j}(k_{1x}(x-\frac{a}{2}))} \times e^{-\text{j}(k_{1y}(y-\frac{b}{2}))} \quad (27)$$

where $\tilde{p}_{\text{inc}}$ is the amplitude and phase of the incident plane wave. The variables k_{1x} and k_{1y} are the projections of the wave vector k_1 and are given by:

$$\begin{aligned} k_{1x} &= k_1 \sin(\theta)\cos(\varphi) \\ k_{1y} &= k_1 \sin(\theta)\sin(\varphi) \end{aligned} \quad (28)$$

where k_1 is the wave number, that is a relation between the frequency ω and the sound celerity into the exciting fluid c_1, given by:

$$k_1 = \frac{\omega}{c_1} \quad (29)$$

Remembering Eq. (25) the generalized force vector due to the incident pressure field $\tilde{P}_{\text{inc}}(x,y)$ can be written as:

$$\{\tilde{\mathbf{F}}_w\} = \int_0^a \int_0^b \tilde{P}_{\text{inc}}(x,y)\{\phi_w(x,y)\}\text{d}y\text{d}x \quad (30)$$

The computation of this integral is cumbersome once that the pressure field generated by the incident plane wave given in Eq. (27) has exponential terms that are frequency dependents and imaginary. To overcome this issue Loredo et al. (2011) propose an alternative way to calculate the generalized forces vector:

$$\{\tilde{\mathbf{F}}_w\} = 2\,\tilde{p}_{\text{inc}}\{\tilde{\Psi}(\mathbf{k_1})\} \quad (31)$$

where the vector $\{\tilde{\Psi}(\mathbf{k_1})\}$ is a $m \times n$ column vector that may be written as:

$$\{\tilde{\Psi}(\mathbf{k_1})\} = \begin{Bmatrix} I_x^1(k_{1x}) I_y^1(k_{1y}) \\ \vdots \\ I_x^p(k_{1x}) I_y^q(k_{1y}) \\ \vdots \\ I_x^m(k_{1x}) I_y^n(k_{1y}) \end{Bmatrix} \quad (32)$$

where $I_x^p(k_{1x})$ and $I_y^q(k_{1y})$, for the adopted basis functions, are given by the following integrals:

$$\begin{aligned} I_x^p(k_{1x}) &= \int_0^a e^{-\text{j}(k_{1x}(x-\frac{a}{2}))} \sin\left(\frac{p\pi x}{a}\right)\text{d}x \\ I_y^q(k_{1y}) &= \int_0^b e^{-\text{j}(k_{1y}(y-\frac{b}{2}))} \sin\left(\frac{q\pi y}{b}\right)\text{d}y \end{aligned} \quad (33)$$

The vector $\{\tilde{\Psi}(\mathbf{k_1})\}$ can be now implemented using the following recurrence:

$$\begin{aligned} I_x^p(k_{1x}) &= \frac{p\pi a[e^{(\text{j}k_{1x}\frac{a}{2})} - (-1)^p e^{(-\text{j}k_{1x}\frac{a}{2})}]}{(p\pi)^2 - (k_{1x}a)^2} \\ I_y^q(k_{1y}) &= \frac{q\pi b[e^{(\text{j}k_{1y}\frac{b}{2})} - (-1)^q e^{(-\text{j}k_{1y}\frac{b}{2})}]}{(q\pi)^2 - (k_{1y}b)^2} \end{aligned} \quad (34)$$

2.5 - Vibroacoustic Indicators

It is assumed light fluid for the two sides of the plate, and with this assumption, the sound power can be calculated from the far-field (hemisphere with infinite radius) sound pressure distribution, in contrast with the near-field (field very close to the sound source) hypothesis, once that the pressure distribution at the surface is not needed. With this assumption the acoustic pressure in the receiving fluid can be calculated at point (r,θ,φ) by the simplified Rayleigh's integral as proposed by Loredo et al. (2011):

$$\tilde{P}_2(r,\theta,\varphi)=\frac{-\omega^2\rho_2 e^{jk_2 r}}{2\pi r}\hat{w}(k_{2x},k_{2y}) \quad (35)$$

where ρ_2 is the receiving fluid density and the variables k_{2x} and k_{2y} are the projections of the wave vector k_2 and are given by:

$$\begin{aligned} k_{2x}&=k_2\sin(\theta)\cos(\varphi)\\ k_{2y}&=k_2\sin(\theta)\sin(\varphi)\end{aligned} \quad (36)$$

where k_2 is the wave number, that is a relation between the frequency ω and the sound celerity into the receiving fluid c_2, given by:

$$k_2=\frac{\omega}{c_2} \quad (37)$$

The variable $\hat{w}(k_{2x},k_{2y})$ is the double Fourier transform of the plate's displacement and can be written as:

$$\hat{w}(k_{2x},k_{2y})=\int_0^a\int_0^b \tilde{w}(x,y)e^{-j(k_{2x}(x-\frac{a}{2}))}\times e^{-j(k_{2y}(y-\frac{b}{2}))}\mathrm{d}y\mathrm{d}x \quad (38)$$

The transverse displacement $\tilde{w}(x,y)$ in Eq. (38) can be calculated using Eq. (15). Moreover, if we look the similarities between Eq. (38) and Eq. (27) the double Fourier transform of the plate displacement can be calculated like the generalized forces vector due to a plane wave excitation, being defined as:

$$\hat{w}(k_{2x},k_{2y})=\{\widetilde{\mathbf{A}}\}\{\tilde{\Psi}(\mathbf{k_2})\} \quad (39)$$

where $\{\widetilde{\mathbf{A}}\}$ is the coefficient vector of the transverse displacement and $\{\tilde{\Psi}(\mathbf{k_2})\}$ is an auxiliary vector like the one defined in Eq. (31), but considering the wave number of the receiving fluid. The radiated acoustic pressure, and according with the far-field hypothesis, can be calculated by the integration of the radial intensity over a hemisphere of infinite radius:

$$W_{\mathrm{t}}=\frac{\rho_2\omega^4}{8c_2\pi^2}\int_0^{2\pi}\int_0^{\frac{\pi}{2}}|\hat{w}(k_{2x},k_{2y})|^2\sin(\theta)\mathrm{d}\theta\mathrm{d}\varphi \quad (40)$$

Considering that the system is excited by a plane wave, the preceding equation gives the radiated acoustic power for this plane wave which allows to define an oblique incidence transmission coefficient $\tau(\theta,\varphi)$, given by:

$$\tau(\theta,\varphi)=\frac{W_{\mathrm{t}}(\Pi_{\theta,\varphi})}{W_{\mathrm{inc}}(\theta,\varphi)} \quad (41)$$

where $W_{\mathrm{inc}}(\theta,\varphi)$ is the incident power of this plane wave, that may be written as:

$$W_{\mathrm{inc}}(\theta,\varphi)=\frac{|\tilde{p}_{inc}|^2\cos(\theta)S}{2\rho_1 c_1} \quad (42)$$

where S is the plate area. Defined the incident acoustic power and the radiated acoustic power it is possible to define the acoustic transparency of the plate, by the relation between these two quantities. This relation is known by transmission loss (TL) and can be written as:

$$\mathrm{TL}=10\log\left(\frac{W_{\mathrm{inc}}(\theta,\varphi)}{W_{\mathrm{t}}(\Pi_{\theta,\varphi})}\right) \quad (43)$$

The transmission loss is an important indicator of the treatment effectiveness once that represents the fraction of the incident acoustic power that isn't radiated to the receiving fluid. In addition to the transmission loss, others indicators can be defined like the mean square velocity that is defined as a space and time average of the structure velocity and can be written as:

$$\langle V^2 \rangle = \frac{1}{S}\int_0^a \int_0^b \frac{1}{2}\left|\frac{d\tilde{w}(x,y)}{dt}\right|^2 \mathrm{d}y\mathrm{d}x \quad (44)$$

The preceding equation can be rewritten, taken into account Eq. (15), as:

$$\langle V^2 \rangle = \frac{\omega^2}{2S}\{\tilde{\mathbf{A}}\}^{\mathrm{T}}\left[\int_0^a \int_0^b \{\phi_w(x,y)\}\{\phi_w(x,y)\}^{*\mathrm{T}}\mathrm{d}y\mathrm{d}x\right]\{\tilde{\mathbf{A}}\}^* \quad (45)$$

where * represents the complex conjugate operation. As was said, the mean square velocity represents the space and time average of the structure velocity. Taken into account its definition, a new vibroacoustic indicator can be defined as only the time average of the structure velocity and can be defined as:

$$\langle V^2(x,y) \rangle = \frac{\omega^2}{2S}\{\tilde{\mathbf{A}}\}^{\mathrm{T}}\{\phi_w(x,y)\}\{\phi_w(x,y)\}^{*\mathrm{T}}\{\tilde{\mathbf{A}}\}^* \quad (46)$$

The square velocity is an indicator that is appropriated to a 2D representation of the time average of structure velocity at a given frequency. Another indicator that gives an idea of the treatment efficiency is the radiation efficiency and is defined as a non-dimensional ratio between the radiated sound power and the mean square velocity of the plate:

$$\sigma = \frac{W_t}{\rho_2 c_2 S \langle V^2 \rangle} \quad (47)$$

Considering the above definitions, the radiation efficiency expresses the portion of vibration energy transformed into sound.

3- VALIDATION AND EVALUATION

In order to validate and evaluate the mechanical and vibroacoustic model, their main characteristics are studied in this section.

3.1 - Basis Dimension and Degrees of Freedom

In the Rayleigh-Ritz method the dimension of the trial functions space it's a matter of great importance. As well as the finite elements give the representativeness of the model in the finite element method, the dimension of the basis functions in the Rayleigh-Ritz method determines the structure discretization. With this model, the displacement field is builded with five different unknowns which leads to a model with $(5\times m\times n)$ degrees of freedom, where m and n are the maximum orders of the trial functions in x and y-direction, respectively. If we consider the finite element method, different calculations are needed to estimate the total number of degrees of freedom once that it depends on the mesh but a comparison with a simply-supported plate performed in the software Actran® was made. For this, the magnitude of a frequency response function (receptance) of a simply-supported plate with the properties shown in Table 1 was studied. The frequency response function calculated with the software Actran® was performed using the element "HEX08" that is a solid element with 3 degrees of freedom per each node. The use of 1344 elements led to a model with 6525 degrees of freedom. The excitation is a point force applied at $x = 0.08$ m and $y = 0.07$ m from the origin.

Table 1 – Geometric and mechanical plate properties.

a (m)	b (m)	h (mm)	E (GPa)	ρ (Kg/m^3)	ν	η
0,48	0,42	3,22	66	2680	0,33	0,005

With the present model an 8×8 order for the basis functions is adopted which leads to a model with 320 degrees of freedom.

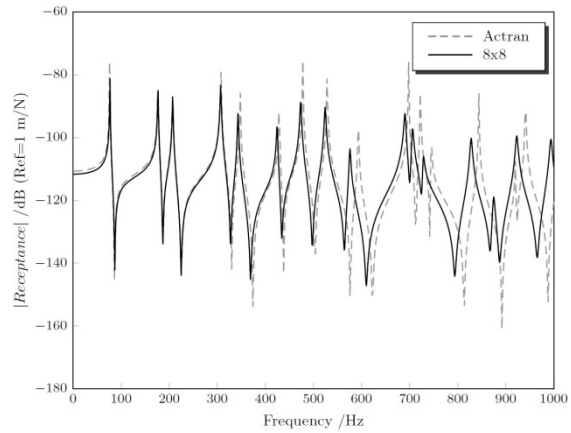

Fig. 5 – Comparison between the present model with an 8×8 order and Actran®.

The comparison between the present model and the frequency response function obtained with the software Actran® in Fig.5 show a good agreement between the two models, particularly at low frequencies. As the frequency increases the model studied in this work is more damped and underestimate the natural frequencies relatively to Actran®. Considering that the present model uses a plate theory that considers the effect of the shear stress is acceptable that it tends to underestimate the natural frequencies. It can be said that these results are excellent if we take into account that the two models are completely different, once that in the Actran® a solid finite element is used in contrast with the present work, where is used a plate theory and the Rayleigh-Ritz method. Besides that, the Actran® example was performed with 6525 degrees of freedom against 320 used with the present model, which is an overwhelming difference of 6205 degrees of freedom.

3.2 - Multilayer Behavior

As was said in the presentation of the structural model, a linear displacement field across the thickness is used, where the displacement continuity is enforced at each interface. Here a graphical representation of the displacement in x-direction across the thickness is done to show the multilayer behavior despite the enforced shear stress continuity. For that, a three layer laminate is studied and its properties are shown in Table 2.

Table 2 – Geometric and mechanical laminate properties.

Layer	a (m)	b (m)	h (mm)	E (GPa)	ρ (Kg/m^3)	ν
1	0,48	0,42	3	210	7800	0,3
2	0,48	0,42	2	66	2680	0,33
3	0,48	0,42	1	210	7800	0,3

The displacement was calculated for a distributed pressure of 10^5 Pa and considering a simply-supported plate, the displacement field across the thickness, in the center of the plate ($x=0,24$ mm and $y=0,21$ mm), can be seen in Fig. 6.

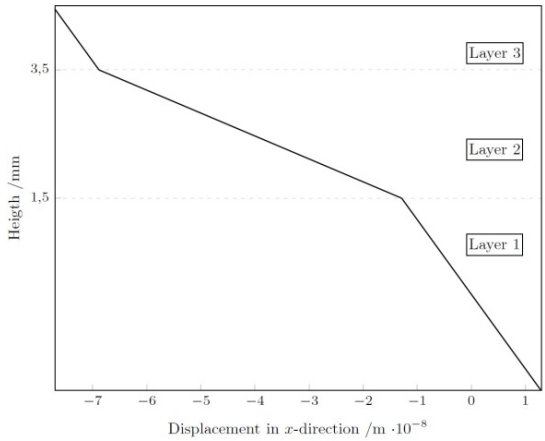

Fig. 6 – Displacement in x-direction for a distributed pressure of 10^5 Pa

It can be seen in Fig. 6 that the displacement continuity at each interface was ensured as well as the multilayer behavior despite the displacement of a generic layer ℓ can be written as a function of the displacements of the first layer. In addition, it can be said that the displacement field across the thickness is the expected one, once that the slopes (deformation - $\mathrm{d}u/\mathrm{d}x$) of the first and third layers are equal and smaller than that of the second layer. This reflects the fact that the first and third layers are steel layers and the second one is an aluminum layer with lower Young's modulus.

3.3 - Vibroacoustic Indicators and Patches Handling

In order to validate the model implementation and obtained results in terms of vibroacoustic indicators, a comparison with the results obtained by Loredo et al. (2011) was done. The considered plate is immersed in air and receiving an acoustic excitation of an incident plane wave with unitary amplitude and incidence angles of $\theta=85^\circ$ and $\varphi=0^\circ$. The geometric and mechanical properties of the studied plate can be seen in Table 3.

Table 3 – Geometric and mechanical Loredo's (2011) plate properties.

a (m)	b (m)	h (mm)	E (GPa)	ρ (Kg/m^3)	ν	η
0,455	0,376	1	210	7800	0,3	0,01

In the work performed by Loredo et al. (2011) the properties of the exciting and receiving fluid are not given but in this work the properties of the air at 25ºC are assumed, once that is the temperature considered for the properties of the viscoelastic layer. The referred properties can be seen in Table 4.

Table 4 – Exciting and receiving fluid properties - Air (T=25ºC).

Fluid	Sound Celerity ($m.s^{-1}$)	Density ($Kg.m^{-3}$)
Exciting/Receiving	346,13	1,1839

The vibroacoustic indicators were obtained for three different cases. Firstly, for the base plate alone and then a total and a partial treatment were applied. In the viscoelastic treatments, the constraining layer is also considered to be made with the same steel of the base layer, and thickness is set to 0,5mm. The viscoelastic layer has a thickness of 0,25mm and the material is the 3M ISD112. A constitutive law for the storage modulus and loss factor for this material is given in A. Castel et al. (2012) and is shown in Eq. (48) and (49), however only discrete values for some frequencies of these properties are given in Loredo et al. (2011) and there is no certainty that the constitutive law used for all the frequency range is the same. In these studies, is considered a Poisson's ratio of 0,45 and a density equal to 1140Kg/m^{-3} for the viscoelastic material.

$$E'(\omega) = 10^{(0.4884\log(\omega)+5.3848)} \tag{48}$$

$$\eta(\omega) = 10^{(-0,0175\log(\omega)^3+0,0571\log(\omega)^2+0,0015\log(\omega)-0,0874)} \tag{49}$$

The partial treatment applied covered 40% of the total plate area and was added in the central region with the dimensions of 288×238 mm. Here, for practical reasons, it was used a maximum order of 6 for the x and y-directions whereas in the work developed by Loredo et al. (2011) was used a maximum order of 13 for both directions. The frequency range varies only between 0 and 700Hz which is a smaller frequency range but that changes nothing about the targets of this study. The obtained mean square velocity is depicted in Fig. 7 and the result obtained by Loredo et al. (2011) can be seen in Appendix. Analyzing Fig. 7, it can be seen that, in general and for the studied frequency range, a good match is obtained with the result available in Appendix. Furthermore, it should be noted that the properties of the fluid are not given in the work developed by Loredo et al. (2011) and only discrete values of the storage modulus and loss factor of the viscoelastic material for some frequencies are given. Analyzing the obtained vibroacoustic indicator from a more particular point of view some important aspects should be noted. Firstly, both total and partial treatment makes the plate more efficient in a vibroacoustic viewpoint once that at the resonance frequencies the values of the mean square velocity decreased. This capability to improve the behavior of the structure in the resonance zones is achieved either with the total treatment as the partial treatment, yet this fact is most remarkable in the total treatment. However, this result is particularly interesting once that with a smaller structural modification and with less added mass similar results to those of a total treatment can be achieved.

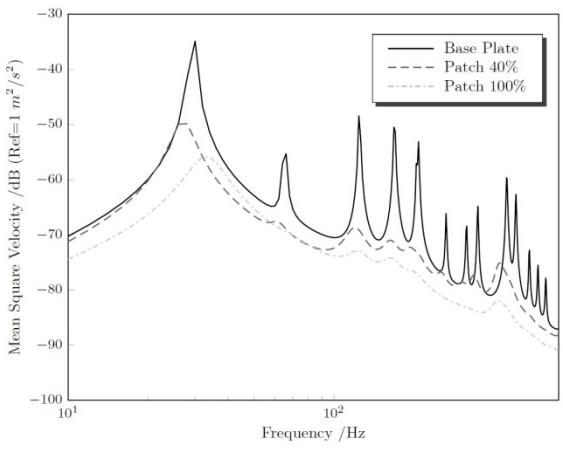

Fig. 7 – Mean square velocity for three different configurations.

4 - ANALYSIS OF CONSTRAINED-LAYER DAMPING PATCHES

It is well known that the use of damping patches enables a high damping capability with a smaller structural modification but the results obtained in the model validation raise interesting questions about the optimal covered area or the correct positioning of the patches, for example. To answer these questions is important to establish an objective because an optimal solution always depends on the proposed target. However, the intent of this work is to show some vibroacoustic indicators in order to analyze the main ideas about the changes caused by different treatment's configurations establishing a commitment between damping capability and added mass.

4.1 - Covered Area

In Fig. 8 five different covered areas (0, 20, 40, 60, 80 and 100%) by a rectangular central patch with the same relation length to width that the base layer are depicted. The geometric and mechanical properties of the structure are the same as those from the validation of the vibroacoustic indicators and patches' handling (see Table 3 and 5) as well as the fluid properties from Table 4 and basis functions.

Table 5 – Geometric and mechanical of Loredo's (2011) patch treatment.

Layer	h (mm)	E (GPa)	ρ (Kg/m^3)	ν	η
2	0,25	Eq. (48)	1140	0,45	Eq. (49)
3	0,5	210	7800	0,3	0

It is clear that with the increase in the covered area the transmission loss increase, proving the treatment's efficiency. It is interesting to note that for a covered area of 20 and 40% the peaks in the transmission loss are shifted to left in the frequency axis (influence of the added mass) whereas for the covered areas of 80 and 100% the peaks are shifted to right (influence of the added stiffness).

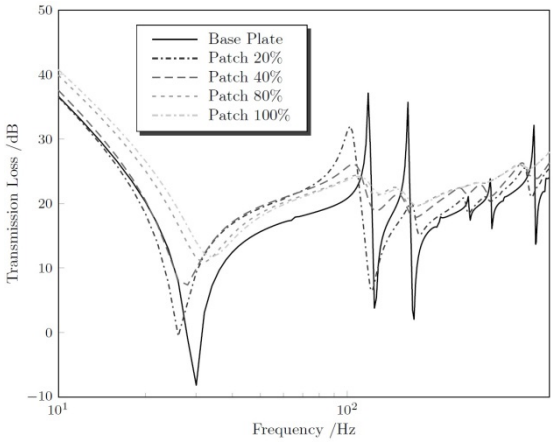

Fig. 8 – Transmission loss for different configurations.

It is worth to mention that the differences in transmission loss between a 80% covered area by a central patch and a total treatment can be considered almost negligible which proves that a high damping capability can be achieved with a smaller structural modification. Even the central patch covering 40% of the total area shows a high damping capability, relatively to the base plate alone, with half the added mass of the central patch covering 80% of the total area.

4.2 - Analysis of Patches Distributions

Considering the great advantage of this model with the patches' handling, different distributions of covered area can be tested to improve the structure performance. An interesting approach could be reduce the vibration energy of a given mode, which can be achieved placing the viscoelastic patches in a strategic area where the shear deformation is imposed to the viscoelastic layer. In Fig. 9 the mode shape (1,3) and a suggested patch treatment to decrease the energy of this respective mode in depicted.

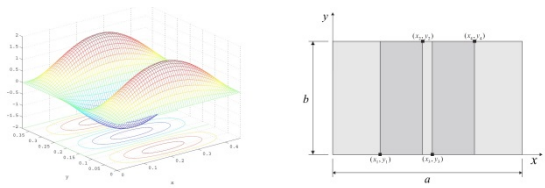

a) Mode (1,3) b) Patches

Fig. 9 – Example of selective damping for mode (1,3).

The two strips in Fig. 9b were defined to take advantage of the phase opposition in

the mode shape (1,3) forcing shear deformation in the viscoelastic layer and so improve the damping capability. The geometrical properties of the patches that define the integration limits for the structural matrices generation can be seen in Table 6. All the remaining properties are the same to those used in the previous analyzes and the total covered area is equal to 40% of the base plate area.

Table 6 – Geometrical properties of patches distributions.

Treatment	Length (m)			
	x_1	x_2	x_3	x_4
Strips (1,3)	0,1332	0,2242	0,2309	0,3219
Treatment	Width (m)			
	y_1	y_2	y_3	y_4
Strips (1,3)	0	0,3760	0	0,3760

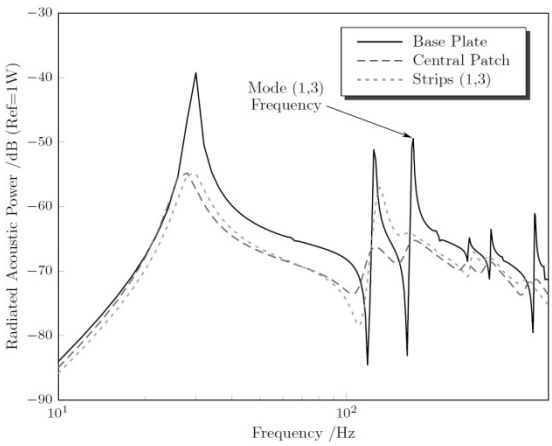

Fig. 10 – Radiated Acoustic power for different patches configurations.

Analyzing Fig. 10, where the radiated acoustic power is presented, it can be seen that at the frequency of the natural mode (1,3) the considered patch treatment nullifies that particular resonance. However, it is important to remember that this result is achieved with corresponding higher values for the radiated acoustic power at other frequencies in the considered range. With the same covered area, it seems that the central patch is the best commitment considering all the frequency range.

5- CONCLUSION

The passive damping by viscoelastic patches is an efficient mean for the noise and vibration control of structures. The main advantage of the presented mechanical model is that the number of degrees of freedom is independent of the number of layers, avoiding very cumbersome models. In addition, an efficient patch handling is achieved, comparative to the finite element method taking advantage of the Rayleigh-Ritz method and its globally defined basis functions. In the analysis of constrained-layer damping patches it was seen that the 40% covered area by a central patch seems to be a good commitment between damping capability and added mass. Then, the analysis of patches distributions served to show that a selective damping can be achieve taking advantage of the phase opposition for a given mode, forcing the viscoelastic layer to shear deformation. All the results show that a structure can be efficiently damped by adding appropriate patches. However, the difficulty to have the better damping consists first to choose the appropriate viscoelastic treatment and second to determine the better distribution while keeping the best ratio performance/added mass.

6- APPENDIX

Vibroacoustic Indicators – Loredo et al. (2011)

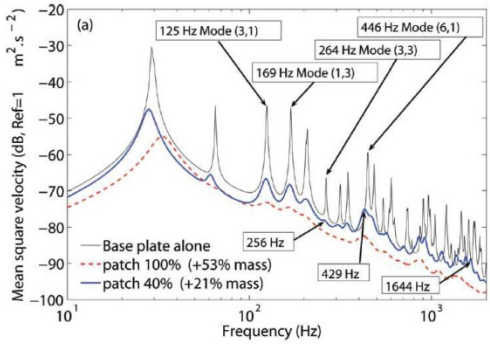

Fig. 11 – Mean square velocity for three different configurations – Loredo et al. (2011).

7- REFERENCES

Guyader, J.L. and Lesueur, C. 1978. Acoustic transmission through orthotropic multilayered plates, part I: Plate vibration modes, Journal of Sound and Vibration, 58 (1), p. 51-68.

Woodcock, Roland L., 2008. Free vibration of advanced anisotropicmultilayered composites with arbitrary boundary conditions, Journal of Sound and Vibration, 312 (2008), p. 769-788.

Loredo, A., Plessy, A. and Hafidi, A.E. 2011. Numerical vibroacoustic analysis of plates with constrained-layer damping patches, Journal of Acoustical Society of America, 129 (4), p. 1905-1918.

Castel, A., Loredo, A., Hafidi, A. El and Martin, B. 2012. Complex power distribution analysis in plates covered with passive constrained layer damping patches, Journal of Sound and vibration, 331 (2012), p. 2485-2498.